

# **MODELING OF FILM VAPORIZATION AND FILM BOILING INSIDE AN ENGINE CYLINDER**

**Chia-fon F. Lee, Rajan K. Kapadia and Steve T. Chin**  
**Department of Mechanical and Industrial Engineering**  
**University of Illinois at Urbana-Champaign**  
**Urbana, IL 61801**

## **INTRODUCTION**

Engine-out HC (hydrocarbon) emissions resulting from liquid fuel, which escapes from the combustion process, provides the motivation to better understand the film vaporization in a combustion chamber. Previous works theorized that the removal of liquid fuel from the combustion cycle was a result of the film boiling regime of the film boiling curve, otherwise known as the Leidenfrost phenomenon. The objective of this work was to develop a robust film boiling model, which incorporated the effects of increased acceleration on film boiling, and consequently, on film vaporization at high temperatures.

New film boiling correlations which encompassed increased acceleration effects for the nucleate boiling regime and the film boiling regime were investigated, implemented, and validated. Validation was conducted using published experimental data sets for film boiling heat flux from the surface to the film. It was observed that a noticeable increase in heat flux was a result of increased acceleration for films in saturated film boiling in both nucleate and film boiling.

Computational simulations were conducted using a semi-infinite plate and a direct-injection spark-ignition (DISI) engine. The semi-infinite plate provided a controlled environment which could separate the effects of pressure and acceleration on film boiling heat flux, film vaporization rates, and film vaporization times. The effect of decreased film vaporization rates, during the Leidenfrost phenomenon, was observed to decrease with increasing acceleration.

Finally, the DISI engine computations were conducted. The multicomponent film vaporization model were then used to simulate the hydrocarbon emissions resulting from wall-wetting in gasoline engines. Qualitative comparisons between the computed and measured results were made. The agreement of both the overall trends and the transient history were reasonable. The computed results also provide insight into the causes of HC emissions. It was revealed that wall-wetting location has a significant effect on HC emissions by allowing some of the unburned HCs an easy access to the exhaust, while making it nearly impossible for others to escape into the exhaust. The wetting of the cylinder liner underneath the exhaust valves and the piston top resulted in large increases in HC emissions. Injection timing affects the amount of film that survived past the combustion process. As film survived into the expansion and the exhaust stroke, the film's composition gradually shifted toward its heavier components and this new composition controls the vaporization characteristic of the film. The new film boiling models were also used to provide the film boiling and film vaporization rates for engine fuel films at temperatures above saturation temperature. As a result of this work, a film vaporization model incorporating the effects of film boiling has been developed. The improved model will allow for the accurate study of film vaporization under boiling conditions which typically occur within the engine combustion chamber.

## **MATHEMATICAL MODEL**

### **Nucleate Boiling Regime Sub-Model**

The nucleate boiling regime is composed of three aspects: the onset of nucleate boiling, the nucleate boiling heat flux, and the critical heat flux point. The onset of nucleate boiling was based on the analysis of an ideal cavity, which Whalley [1] defined as one that is conical in shape with a circular opening. Using the Clausius-Clapeyron equation to model the slope of the vapor pressure curve and then integrating to find the superheat of nucleation and hence the onset of nucleate boiling.

The nucleate boiling heat flux correlation was chosen as it provided the most accurate correlation of the existing experimental data, without ignoring the impact of other effects such as wettability and pressure. The final form of the correlation is:

$$q_{TS}'' = \left[ 0.16 * \text{Pr}^{\frac{1}{3}} \left( \frac{g\beta k_l^3}{\nu_l^2} \right)^{\frac{1}{3}} (\Delta T_{sat} + \Delta T_{sub})^{\frac{4}{3}} \left( \frac{a}{g} \right)^{\frac{1}{3}} \right] + \left[ 2.39 \times 10^6 \text{Pr}^{-4.1} * \left( \frac{k_l (\Delta T_{sat} + \Delta T_{sub})}{\sqrt{\sigma g_o / g (\rho_l - \rho_v)}} \right) * \left( \frac{c_{pl} (\Delta T_{sat})}{h_{fg}} \right)^2 \right] \quad (1)$$

The resulting correlation has a dependence on acceleration of  $a^{1/3}$ . To validate the correlation, simulations were conducted using a semi-infinite plate. The mesh was composed of 5000 cells of uniform dimension. In order to isolate the effects of film vaporization and film heat flux, a film was directly placed on the surface of the plate, forming a 10 micron thick film. Computational results are validated against the data from Merte and Clark [2] and Costello and Tuthill [3]. The computational results fell within experimental error and show good agreement with the data.

A correlation for the superheat of the critical heat flux does not exist. Instead, correlations for the amount of critical heat flux were available [4]. From the critical heat flux correlation, one can derive the critical heat flux point.

### Film Boiling Regime Sub-Model

Two aspects of the film boiling regime that need to be considered are: the minimum heat flux or Leidenfrost point and the film boiling heat flux. Minimum heat flux can be calculated from the solution of the transient conduction equations for intimate contact between two infinite slabs.

Of the available film boiling heat flux expressions reviewed, Klimenko's expressions [5] seemed best at providing the accuracy sought in modeling increased acceleration fields and is used in the current work. Since the flow in the vapor layer of the piston top film was determined to be laminar, the Reynolds analogy was used. The resulting heat flux correlation is

$$q_{TS}'' = 0.19 \Delta T_{sat} \left( \frac{\rho_v (\rho_l - \rho_v) a c_{pv} k_v^2}{\mu_v} \right)^{1/3} 0.89 \left( \frac{h_{fg}}{c_{pv} \Delta T_{sat}} \right)^{1/3} \quad (2)$$

The acceleration dependence is given as:  $a^{1/3}$ , which falls directly in the range of the limited experimental film boiling data for increased accelerations. The calculated values the above correlation agree reasonably well with the experimental results of Nakajima et al. [6] and Ogata and Nakayama [7].

### Film Vaporization Sub-Model

Three regimes not yet discussed, but important in defining a full film boiling curve are: non-boiling, single phase, and transitional regimes. The treatment of the first two regimes is a carryover of the film vaporization model of Zeng and Lee [8]. The transition regime was simply modeled as a straight line, on a log-log plot, between the critical heat flux and minimum heat flux points of the film-boiling curve, similar to most published boiling curves. No correlation was implemented for the transition regime, as no established correlation incorporating the effects of pressure or acceleration was available. This is primarily attributed to the unstable nature of the liquid film in this regime.

## RESULTS AND DISCUSSIONS

### Semi-infinite plate results

The semi-infinite plate geometry and injection strategy, previously described, was used to isolate the impact of parameters on film boiling and film vaporization of a pentane film. Numerous simulations

were run varying one or two of the following: wall temperature, acceleration, and/or pressure. In order to reduce any issues with mass diffusion parallel to the surface near boundaries, only the central film parcel was monitored to obtain film vaporization rates. The simulations were ended when the film had completely vaporized. As the film vaporization rate is transient, the peak rate was reported during the simulation.

Results of the film vaporization rate at varied pressures are presented in Fig. 1. These simulations were run at standard acceleration and at pressures of 0.101, 0.201, and 0.301 MPa. Figure 1 shows that increasing the pressure at a constant wall temperature could cause a shift from the film boiling regime to the transition regime. In addition, an increase in pressure is noted to delay the initiation of all three major regimes. This is depicted by the increase in wall temperature necessary to achieve the three major points: onset of nucleate boiling, critical heat flux (CHF in Fig. 1) point, and minimum heat flux (MHF in Fig. 1) point at increasing pressures. Due to the competing effects of increased temperature and pressure on vaporization rate, the expected decrease in vaporization rate with increased pressure alone is not evident. Rather, the temperature effect dominates.

Figure 2 plots the film vaporization rates for varied accelerations at ambient pressure. The accelerations were varied between 0.01, 1, and 100g. Peak vaporization occurred at the critical heat flux point of the nucleate boiling regime, which produced the highest heat flux from the hot surface to the liquid film. As the acceleration increased, the critical heat flux increased, resulting in an increase in the film vaporization rate. The critical heat flux superheat also increased with acceleration while the minimum heat flux temperature remained approximately constant, shortening the transition regime. Finally, the increase in heat flux with acceleration produced an increased vaporization rate throughout the film boiling regime.

### **Engine simulation results**

The engine mesh used in the simulations is the DISI engine created by Chin and Lee [9] with the geometry of the GM Quad-4 engine. The mesh at BDC consists of 55,250 cells. For the simulations conducted in the present work, the engine cycle is operated from -30 to 720 crank angle degrees (CAD), with BDC of the intake stroke at 0 CAD. Cylinder wall temperature and piston top temperature are taken from Li et al. [10,11] and correspond to 388 K and 422 K, respectively.

Figure 3 illustrates the fate of the film evaporating from location EE (on the cylinder liner under the exhaust port). The film that survives the combustion slowly vaporizes throughout the expansion process. Some of the vaporized fuel will undergo oxidation. At EVO, high-pressure, burned gases flow out into the exhaust port carrying with it some of the unburned HC near the exhaust valve. The initial amount of unburned fuel exiting the cylinder is fairly large for location EE. The flows induced by the blowdown process enhance the vaporization of the liquid fuel in the cylinder. Film underneath the exhaust valve is the greatest beneficiary of this process. As the piston starts to move back up, it expels the gases containing the unburned fuel into the exhaust.

Another significant factor affecting HC emissions is the composition of the fuel mixture of the film in the post-combustion stage. Even though the same fuel mixture is injected, the composition of the film is different in the later stages of the cycle. Figure 4 illustrates the variation in the fuel composition with injection timing for wall-wetting of location EE. The initial composition of the spray is shown in the bold line. The other three curves show the compositions of the film at 450 CAD. As the film vaporizes, the lighter components vaporize faster than the heavier components. The composition of the film shifts toward the heavier components, affecting the vaporization rate in the process. The surface temperatures are well above the boiling temperatures of the lighter components, but they are lower than the heavier components such as decane. Once decane is the sole component remaining, the vaporization rate of the film decreases drastically. This increases the probability that the film will not completely vaporize by the end of the exhaust stroke.

Figure 5 plots the film vaporization rates at the two engine speeds during the film lifetime to demonstrate the effects of acceleration on film boiling. The simulations conducted in the present work occur at engine speeds of 1000 and 2000 rev/min, in a non-combusting environment. Negative

accelerations are treated as an acceleration of 0.01 m/s<sup>2</sup> by the film boiling correlations, so that the correlations utilized will not result in values of zero or infinity. Hexane is used as the single component fuel. The trends of the film vaporization curves are consistent with those of the film boiling curves. However, not illustrated in the heat flux curves, the calculation of the vaporization rate at TDC is dominated by the latent heat of vaporization. Although pressure decreases latent heat, the increase in temperature associated with the increase in piston speed dominates and results in a higher latent heat of vaporization for increased piston speeds. This higher latent heat, which is used to calculate heat of vaporization in the non-boiling state, causes an increase in film vaporization rate with increasing engine speeds. At periods of increased acceleration, higher peak film vaporization rates are observed. The second peak in vaporization rate is attributed to the blow-down process that results in a sudden drop in pressure and a reduction of vapor fuel fraction near the film surface. Both enhance the vaporization rate of the film. The icurve flag value in Fig. 5 indicates the regime of film boiling, given as: 0 – non-boiling state, 1 – single-phase boiling regime, 2 – nucleate boiling regime, 3 – transition regime, and 4 – film boiling regime.

### **SUMMARY AND CONCLUSIONS**

A film boiling curve was implemented into KIVA 3V2 [12] to model the effect of the Leidenfrost phenomenon, which is postulated to be the cause of increased vaporization times for fuel films identified as a potential source of engine-out HC emissions. The film boiling curve model was based on validated pool film boiling correlations that incorporated the effects of pressure and acceleration. Subsequently, the film vaporization model [8] was modified to include the effects of film boiling. Computations calculating vaporization rates and times for a 10-micron thick pentane film on a semi-infinite plate under varying pressures and accelerations were conducted. Then, combustion simulations employed the multicomponent film vaporization models were performed to investigate the effects of film vaporization on HC emissions. Finally, simulations of a piston top hexane film in a non-combusting DISI engine were run producing film heat flux and film vaporization rate results. The following conclusions are drawn from this study:

(1) Increases in acceleration result in noticeably increased heat flux for both the nucleate boiling regime and the film boiling regime, in conditions encountered by piston top films. The computations show good capture of the major factors causing the increase.

(2) As acceleration was increased, the Leidenfrost phenomenon had less of an impact in increasing film vaporization times. This was attributed to the increase in film boiling heat flux associated with an increase in acceleration.

(3) The proximity of the wall-wetting location to the exhaust is a key factor in determining the amount of engine-out HC emissions. The location determines whether the unburned fuel exits easily into the exhaust or remains in the cylinder and combusts in the subsequent cycle.

(4) As the film survive into the expansion and the exhaust stroke, the composition of the film tends to shift toward its heavier components as the lighter components quickly vaporize. This new composition affects the vaporization rate of the film.

(5) The transient variation of the film in the engine through many regimes of the film boiling curve point to the importance of the incorporation of all film boiling regimes.

(6) Computational predictions could be further improved by considering the impact of negative accelerations and the impact of fuel effects on film boiling and film vaporization.

### **ACKNOWLEDGEMENTS**

This work was supported in part by the National Science Foundation under grant No. CTS-9734402.

## REFERENCES

- [1] Whalley, P.B., *Boiling, Condensation and Gas-Liquid Flow*, Oxford University Press, New York, 1987.
- [2] Merte, H., Jr. and J.A. Clark, “*Journal of Heat Transfer, Trans. of the ASME*, Vol. 83, pp. 233-242, 1961.
- [3] Costello, C.P., and W.E. Tuthill, *Chem. Eng. Progress Symp.*, Vol. 57, No.32, pp. 189-196, 1961.
- [4] Kutateladze, S.S., *Isv. Akad. Nauk. SSSR, Otd. Tekh. Nauk.*, Vol. 4, p. 529.
- [5] Klimenko, V.V., *Int. Journal of Heat and Mass Transfer*, Vol. 24, pp. 69-79, 1981.
- [6] Nakajima, R., K. Sato, K. Miyaike, M. Kumagai, and Y. Kobayashi, *Heat Transfer in Superconducting Equipment, ASME Heat Transfer Division*, Vol. 299, pp. 39-44, 1992.
- [7] Ogata, H. and W. Nakayama, *Cryogenics*, Vol. 17, pp. 461-470, 1977.
- [8] Zeng, Y. and C. F. Lee, *Journal of Propulsion and Power*, Vol. 16, No. 6, pp. 964-973, 2000..
- [9] Chin, S. T. and C. F. Lee, *Proceedings of the Combustion Institute*, Vol. 29, pp. 767-773, 2002.
- [10] Li, J., R.D. Matthews, R. H. Stanglmaier, C.E. Roberts, and R.W. Anderson, SAE Paper 1999-01-3661, 1999.
- [11] Li, J., Y. Huang, T. F. Alger, R. D. Matthews, M.J. Hall, R.H. Stanglmaier, C.E. Roberts, W. Dai, and R.W. Anderson, ASME Paper 2000-ICE-270, Fuel Injection, Combustion, and Engine Emissions, Vol. 2, ICE-Vol. 34-2, pp. 17-26, 2000.
- [12] Amsden, A., KIVA-3V: A Block-Structured KIVA Program for Engines with Vertical or Canted Valves, Los Alamos Natl. Lab. Rep. LA-13313-MS, 1997.

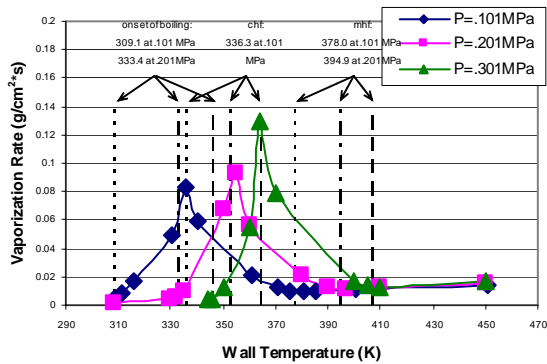


**Figure 1.** Influence of pressure on film vaporization rate.

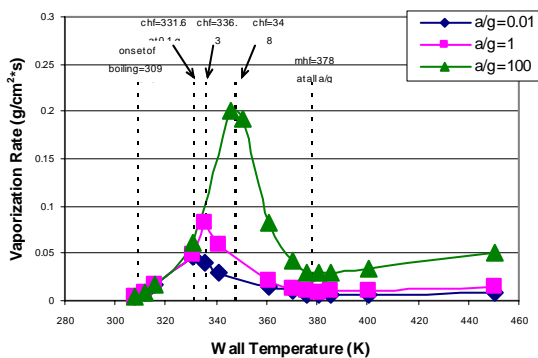


**Figure 2.** Influence of acceleration on film vaporization rate.

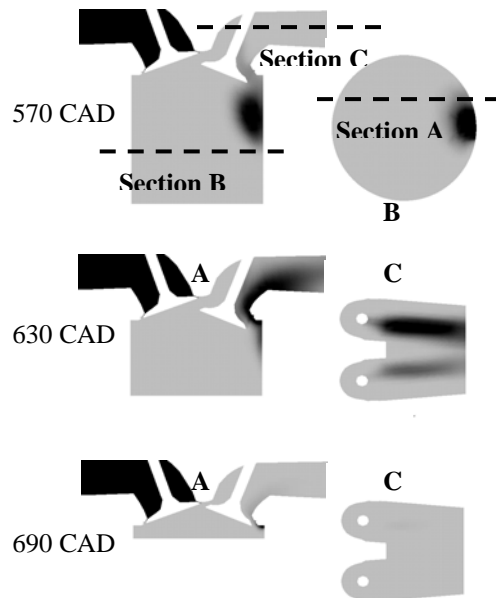


**Figure 3.** Images of wall-wetting of location EE leading to engine-out HC emissions. The gray scale represents the equivalence ratio of the fuel with a maximum value of 0.5.

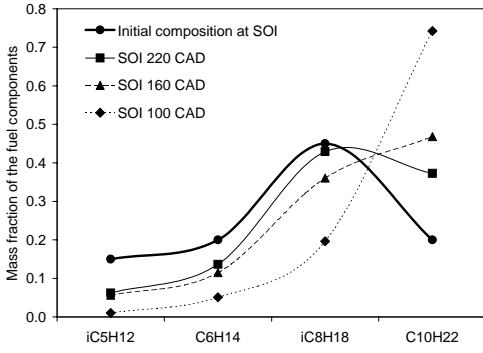


**Figure 4.** Variation in fuel composition of film at 450 CAD with injection timing (all the cases are from wall-wetting of location EE)

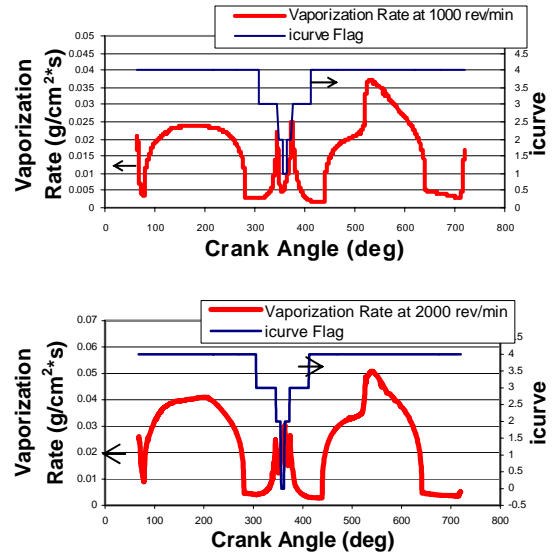


**Figure 5.** Film vaporization rates and icurve flag values from engine at 1000 and 2000 rev/min.